CCFE
CULHAM CENTRE FOR FUSION ENERGY

UK Atomic Energy Authority

UKAEA-CCFE-CP(23)53

A. Shepherd, B. Pouradier-Duteil, T. Patton, A. Rigoni Garola, A. Pimazzoni

Characterization of SPIDER beam homogeneity in caesium using a direct measure of the beamlet current

Characterization of SPIDER beam homogeneity in caesium using a direct measure of the beamlet current

A. Shepherd, B. Pouradier-Duteil, T. Patton, A. Rigoni Garola, A. Pimazzoni

This paper has been submitted to
32nd Symposium on Fusion Technology (SOFT), Dubrovnik, Croatia, 18–23 September 2022

Characterization of SPIDER beam homogeneity in caesium using a direct measure of the beamlet current

A. Shepherd[1,3,a], B. Pouradier-Duteil[2,3], T. Patton[3], A. Rigoni Garola[3], A. Pimazzoni[3]

[1]CCFE, Culham Science Centre, Abingdon, Oxfordshire, OX14 3DB, UK
[2]Ecole Polytechnique Fédérale de Lausanne (EPFL), Swiss Plasma Center (SPC), 1015 Lausanne, Switzerland
[3]Consorzio RFX (CNR, ENEA, INFN, UNIPD, Acciaierie Venete SpA), Corso Stati Uniti 4 – 35127 Padova, Italy
[a]Corresponding author, alastair.shepherd@ukaea.uk

The ITER Heating Neutral Beam (HNB) source prototype SPIDER (Source for the Production of Ions of Deuterium Extracted from a Radio frequency plasma), hosted at the Neutral Beam Test Facility (NBTF) in Padova, Italy, has recently started operating with evaporated caesium in the source. This moves the primary H^- production mechanism from volume to surface processes, increasing the extracted H^- current while decreasing the co-extracted electron current. As in volume operation, the beam exhibits inhomogeneities across the vertical profile due to magnetic drifts, a result of the transverse filter field, which is vital for reducing the electron temperature near the extraction region.

To minimize the occurrence of electrical discharges, SPIDER has been operated with a diminished number of extraction apertures to minimize the vessel pressure/ion source pressure ratio by means of a mask, which reduces the gas flow conductance between the source and the vessel. Therefore, it has been possible to directly measure the current of individual beamlets, due to the increased room between the beamlets, using the non-invasive Beamlet Current Monitor (BCM) diagnostic. Using measurements of five individual beamlets the homogeneity of the SPIDER H^- beam has been assessed, in a range of operating conditions with caesium in the source. The dependence of the beam homogeneity on source parameters (bias, filter field, RF power) has been observed, while increasing the Cs evaporation rate and unbalancing the power of the RF generators have proven to be effective at mitigating the beam inhomogeneity.

Keywords: ITER, SPIDER, NBI

1 Introduction

For large magnetic confinement fusion devices with Neutral Beam Injection (NBI systems), such as ITER, high-energy neutral beams are needed to effectively heat the plasma core. To reach up to 1 MeV of acceleration negative ion beam sources are required, as positive ions have decreasing neutralisation efficiency over 100 keV. The ITER negative ion beam source is under development at the Neutral Beam Test Facility (NBTF) [1], hosted by Consorzio RFX (Padova, Italy), with two experiments: SPIDER and MITICA.

The latter is the full size ITER Heating Neutral Beam (HNB) prototype while SPIDER (Source for the Production of Ions of Deuterium Extracted from RF plasma) is the full-scale ITER ion source [2]. Using the tandem ion source concept devised by IPP, SPIDER has eight RF drivers, paired horizontally with a 200 kW RF generator each, to form the source plasma.

To produce negative ions in sufficient quantities a horizontal filter field is required to separate the hot plasma in the drivers from the colder plasma near the plasma grid (PG), which encloses the ion source. In volume operation, this promotes the formation of vibrationally excited molecular hydrogen in the drivers, which expands towards the PG and undergoes dissociative attachment with cold electrons to form negative ions.

To increase the H^- caesium is evaporated into the source, redistributed by the plasma onto the PG, and forms a low work function surface for the formation of H^- through surface processes [3]. The low electron temperature near the PG then reduces electron detachment, preserving the H^- availability for beam extraction.

Two electrostatic grids downstream of the PG, the extraction grid (EG) and grounded grid (GG) form the negative ion beam on SPIDER. With the GG at ground potential the acceleration grid power supply (AGPS) and extraction grid power supply (ISEG) provide up to -96 kV and -12 kV to the EG and PG respectively, so that the ion source is at -108 kV.

On SPIDER the uniformity of the SPIDER accelerated beam can been studied on the beamlet scale, taking advantage of the reduced number of open PG apertures afforded by the PG mask [4]]. Several SPIDER diagnostics can resolve the beam features on the beamlet scale, including the calorimeter STRIKE [5], beam emission spectroscopy and visible cameras. One recent diagnostic is the Beamlet Current Monitor (BCM) [6], which has measured the beamlet current for five beamlets during the Cs campaign.

Several source parameters have an impact on the homogeneity of the beam. The power of the four RF generators can affect the distribution of the

plasma, while the Cs dynamics influence the generation of H^- at the PG. Additionally, the presence of the filter field creates ExB drifts in the source, which results in a vertical plasma non-uniformity. The biasing of the PG and the bias plate (BP), used to reduce the co-extracted electron current, influences the electric field and thus the drifts. The effect of these parameters is seen in the beamlet current measured by the BCM.

2 Beamlet current monitor

The BCM is a series of five modules, placed downstream of the GG to give the current measurement of five separate beamlets (Figure 1). Each module is mounted to the PG mask pusher support structure by a horizontal plate, which holds the sensor frame in line with the beamlet aperture. Each module consists of a DC sensor with conditioning circuit, an AC sensor and a repeller disk, to suppress backstreaming positive ions (Figure 2).

The DC sensor is a LEM CSTR 0.3p closed loop fluxgate [7]], with a custom conditioning circuit to reduce the sensor offset and increase the gain to around 250 V/A. Shepherd et al have described the BCM DC sensor in more detail in an earlier paper [6].

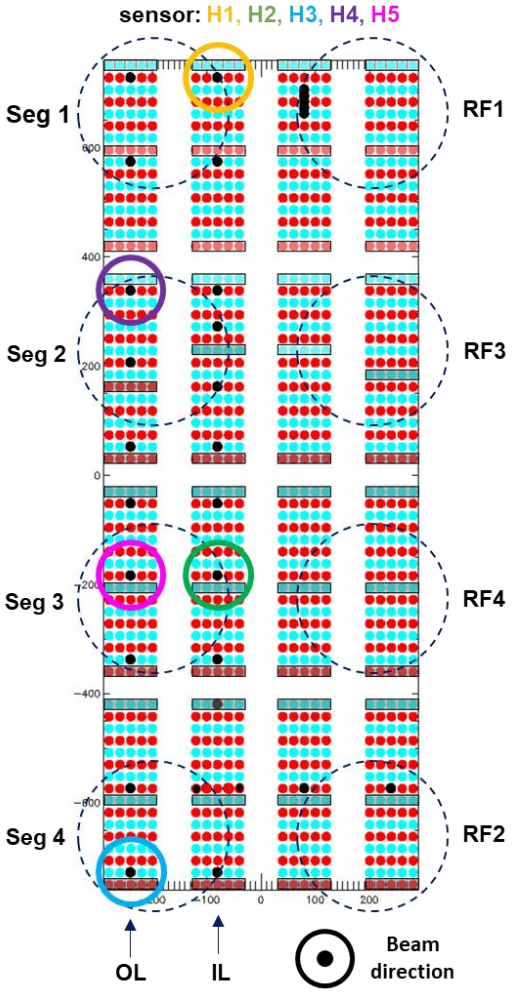

Figure 1. Location of the five beamlet current monitors (solid black circles – open apertures). Projections of RF drivers (dashed circles) and beamlets for the inner and outer left STRIKE tiles (IL and OL) indicated.

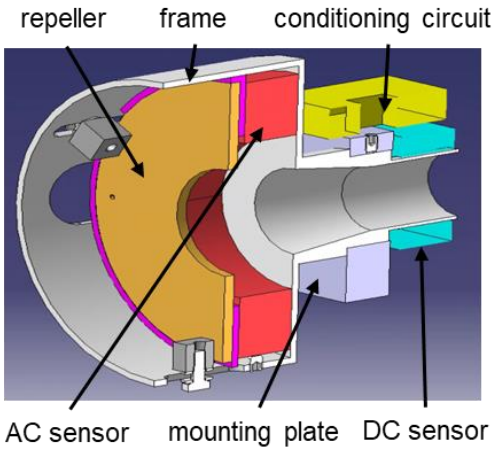

Figure 2. BCM sensor module.

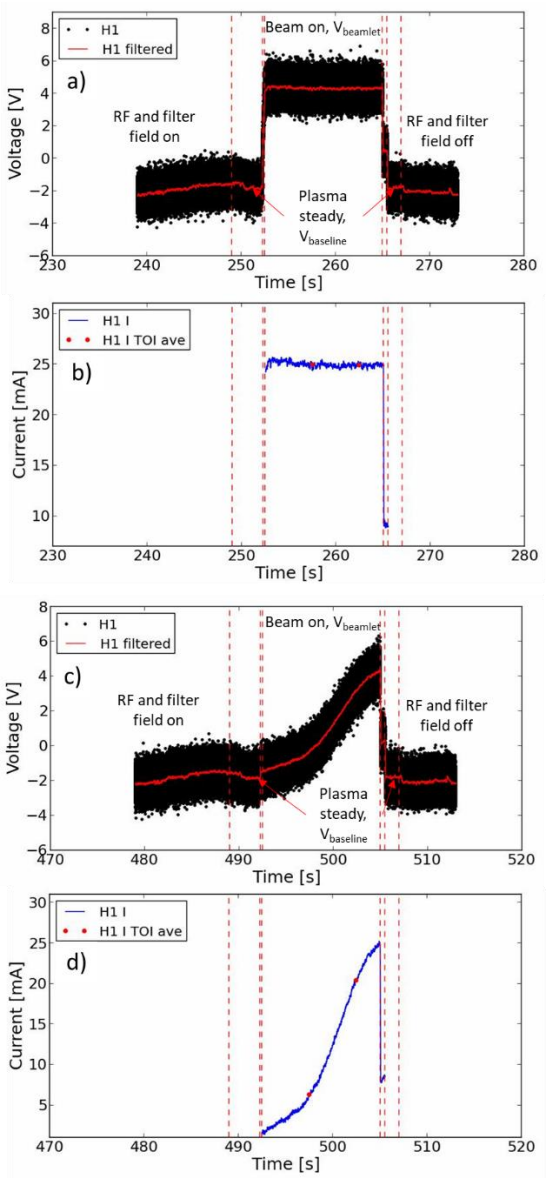

Figure 3. Sensor H1 DC signal analysis for two plasma phases of pulse 9145. a) and c) Raw and filtered sensor voltage for constant and ramped beam voltage. b) and d) calculated beamlet current.

During the 2021 campaign SPIDER was operated with so-called 'macro-pulses', long pulses of up to one hour made up of repeated short plasma

phases, called 'blips', usually lasting less than one minute. The BCM is used for two different types of beam extraction (Figure 3). The first has a constant extraction and acceleration voltage during a single plasma 'blip' to allow a steady beam current for diagnostics that require averaging. The second is a voltage ramp which allows the BCM to measure the Child-Langmuir curve of the beamlet in one plasma 'blip'. In either case the sensor output voltage (black points) is filtered and the voltage baseline taken before and after beam extraction. This is due to the magnetic nature of the sensor making it sensitive to the filter field and plasma. By subtracting the voltage during steady RF power and $I_{PG,}$ $V_{baseline}$, from the voltage during beam extraction, $V_{beamlet}$, the voltage increase due to the beam passing through the sensor is calculated. Using the sensor gain G_s the beamlet current $I_{beamlet}$ is calculated (blue lines) using equation 1.

$$I_{beamlet} = {(V_{beamlet} - V_{baseline})}/{G_s} \qquad (1)$$

3 SPIDER Cs operation

The BCM operated continuously during the SPIDER Cs campaign, measuring current of the five beamlets indicated in Figure 1. The campaign is split into several operational phases, starting with volume operation before moving to the initial ceasiation of the source at 60 kW/generator. The average measured accelerated current density rises from 25 A/m^2 in volume operation to 80 A/m^2 in surface operation (Figure 4) after just several pulses (blip 500), showing the effectiveness of the Cs layer in producing H^- ions.

During this phase studies of the blip repetition rate and caesium injection rate were performed [8]. With the RF power increased to 100 kW/generator the average current increases to 140 A/m^2. Due to limitations on the acceleration grid voltage U_{acc} (50 kV) the best optical conditions, with $U_{acc}/U_{ex} \approx 10$, could not be reached at high power as an extraction voltage U_{ex} > 7 kW is required to extract all of the available negative ions. Therefore, the RF power was decreased to 45 kW/generator to perform parameter scans investigating the beam optics and homogeneity. Lastly, in the campaign the RF power was increased to 100 kW/generator, to test the raising of U_{acc}, followed by operation in deuterium gas instead of hydrogen.

The beamlets display a clear non-uniformity, both vertically and due to their position within the beamlet group. Beamlet H1 (yellow), at the top of the source, is consistently higher than H3 (blue), located at the bottom of the source. In addition, beamlets H2 and H4 (green and pink) often have the highest current, due to them being located in the core of their respective beamlet groups.

The observed inhomogeneity is due to the varying availability of H^- for extraction across the source. A vertical non-uniformity in the negative ion density near the PG has been previously determined in SPIDER using a combination of Langmuir probes and Laser Absorption Spectroscopy [9]. The H^- distribution depends on the distributions of H^+ and e^- in the extraction region, as well as the distribution of the Cs layer on the PG. The magnetic drifts that affect the plasma and Cs transport therefore influence the distribution of H^- density, and thus the beam current.

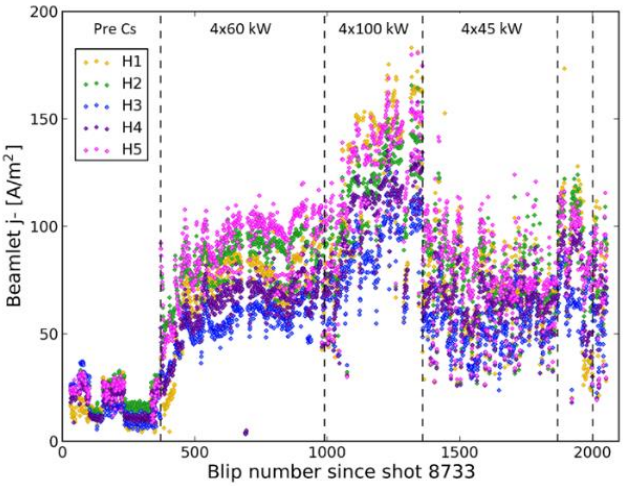

Figure 4. Beamlet current measured by the BCM during SPIDER campaign S21 with Cs. Operational phases separated by dashed lines: Pre Cs (volume operation), Cs operation at 60 kW/generator, Cs operation at 100 kW/generator, parameter scans at 45 kW/generator. HV testing at 100 kW/generator and operation in deuterium in the final two phases.

4 Beam homogeneity

In volume operation, inhomogeneities in the beam current at the beamlet scale have been measured by the STRIKE calorimeter [10]. As well as a general vertical non-uniformity, with a higher current at the top of the source, a non-uniformity on the beamlet group scale has been previously observed. This manifests as a bell shaped profile in the beamlet current, peaking in the centre of the beamlet group, believed to be due to the filter field suppressing the diffusion of the plasma from the drivers. Similar behaviour has been measured by the BCM in volume operation and this paper assesses the inhomogeneity in the beamlet current using the BCM in surface H^- production.

4.1 Extraction voltage

Before attempting to characterise the effect of the biasing and filter field on the beam homogeneity it is important to look at the extraction voltage U_{ex}. Two examples of single blip extraction voltage scans (as in Figure 3c) are shown in Figure 5. The current increases with U_{ex}, following the Child-Langmuir law, until no more H- is available of extraction and the current saturates. The saturation current increases with RF power as the availability of H^- at the PG increases. Until saturation, the extracted currents are similar and the current inhomogeneity low. After the

knee, where the current deviates from the Child-Langmuir law and the perveance is highest, the inhomogeneity increases as the current reflects the distribution of the H^- availability in the source. Care has to be taken to compare points at high U_{ex} so that all the available H^- is extracted when investigating the other source parameters.

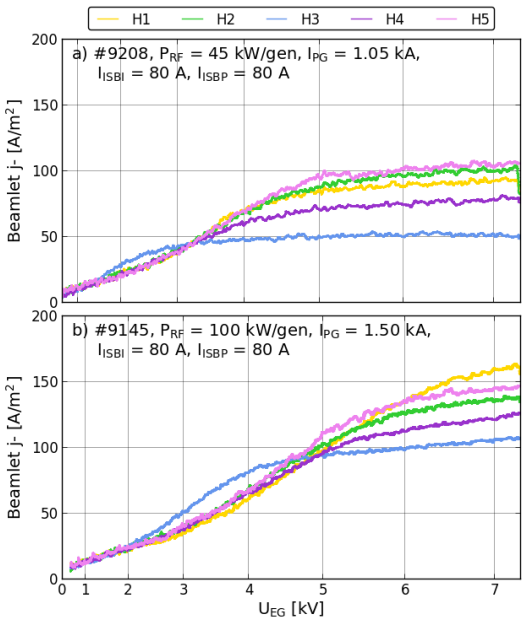

Figure 5. BCM beamlet currents for extraction voltage scans at 45 kW/gen and 100 kW/gen.

4.2 Plasma grid and bias plate biasing

Scans of the bias and bias plate currents were performed at 45 kW/generator, to insure that the acceleration voltage was not limited, negatively affecting the beam optics. Six different combinations of I_{ISBI} and [I_{ISBP}] were investigated, 0 A [0 A, 80 A, 140 A] and 190 A [0 A, 80 A, 140 A], with U_{ex} scans for each. Two such scans are shown in Figure 6.

At U_{ex} = 7 kV all of the beamlets are at saturation and the trend with bias current can be seen (Figure 7). Normalising the currents it is clear that the beamlets decrease proportional to their vertical position, as the bias increases the vertical non-uniformity. The biasing of the PG (I_{ISBI}) has a larger effect on the current than bias plate (I_{ISBP}).

A similar effect can be seen using STRIKE (Figure 8), with the accelerated current decreasing by a factor of two between the top and bottom of the accelerator at high bias. Accompanying the decreased current is a higher divergence as the beamlets are increasingly away from perveance match. It should be noted that the STRIKE measurements were taken at a lower extraction voltage than the BCM reached, as constant U_{ex} and U_{acc} are needed (as Figure 3d). From the U_{ex} scans it is clear that 4.94 kV is not high enough to reach saturation and at low bias is near the knee of the Child-Langmuir curve where the optics is good and the beam uniform, as indicated by the relatively flat current and divergence profiles. However, for showing the large top-bottom non-uniformity at high bias the data is suitable.

Increasing the RF power to 60 kW/ generator and 100 kW/generator gives a similar increase in the top-bottom inhomogeneity (Figure 9), although the distribution appears to be narrowing at higher power.

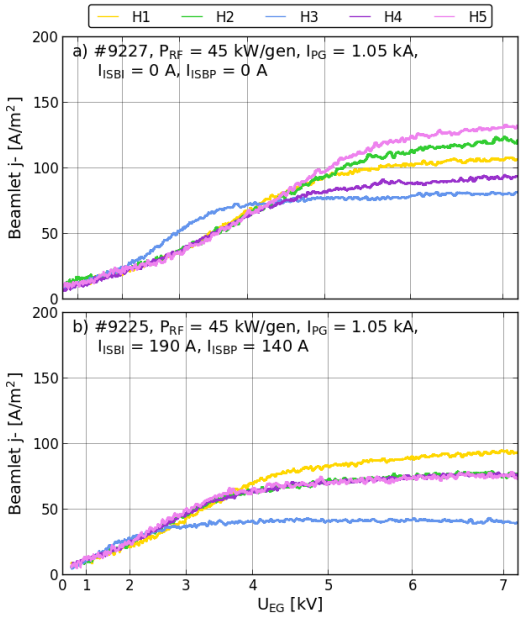

Figure 6. BCM beamlet currents for extraction voltage scans at two different bias and bias plate currents.

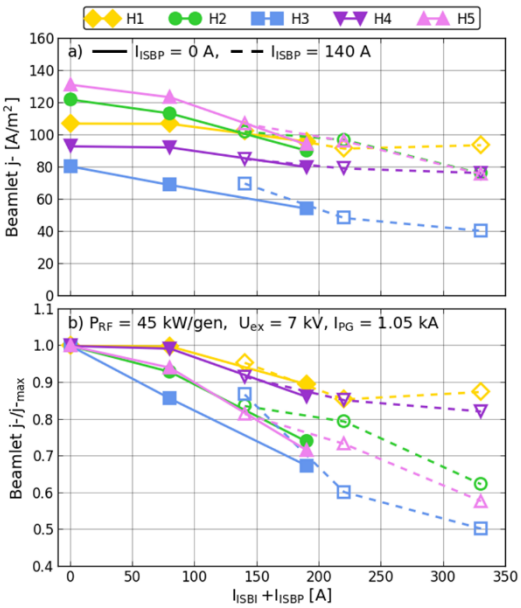

Figure 7. a) BCM beamlet current and b) normalised current, against bias current.

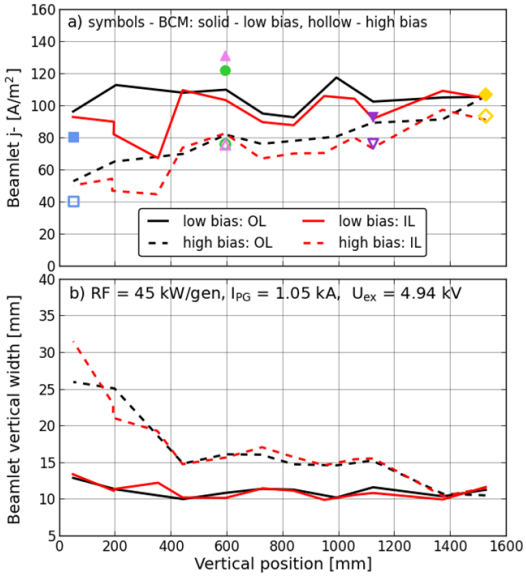

Figure 8. a) STRIKE current and b) beamlet vertical width profiles on the inner (black) and outer (red) left tiles (looking to the source) for high and low bias cases from Figure 7. Compared to BCM currents at 7 kV (coloured markers based on sensor location as in Figure 1). Note that the inner column beamlets near 200 mm and 350 mm are at the edges of the beamlet group, nearest the bias plate, resulting in a low current.

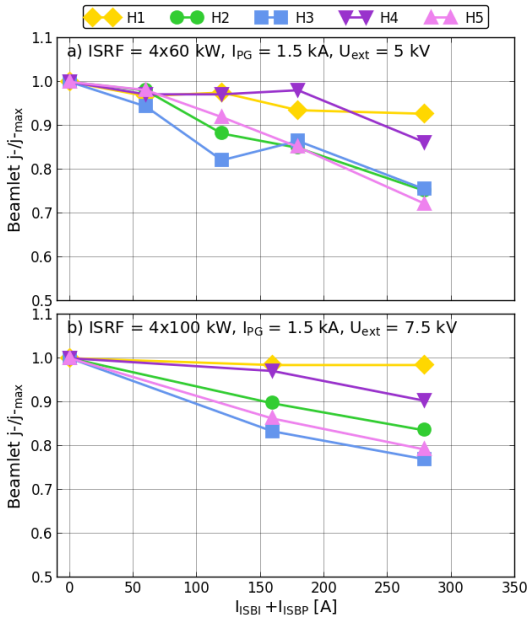

Figure 9. Normalised BCM beamlet currents with increasing bias at a) 60 kW/gen and b) 100 kW/gen.

4.3 Plasma grid current

U_{ex} scans were performed at fixed bias, varying the PG current from 0.9 kA to 1.2 kA (Figure 10). The filter field decreases the current, with the edge beamlets (H1, H3, H4) decreasing more than the core beamlets (H2, H5). This is seen at high extraction voltage where all of the available H- is extracted (Figure 11a). If we take the vertical position of the beamlets relative to the centre of the nearest driver, a composite vertical profile of the beam for one beamlet group is obtained (Figure 11b). With increasing filter field the overall trend is a narrowing of the current profile across the group. Qualitatively this compares with the vertical current profiles measured on STRIKE in both volume [10] and surface operation (Figure 12).

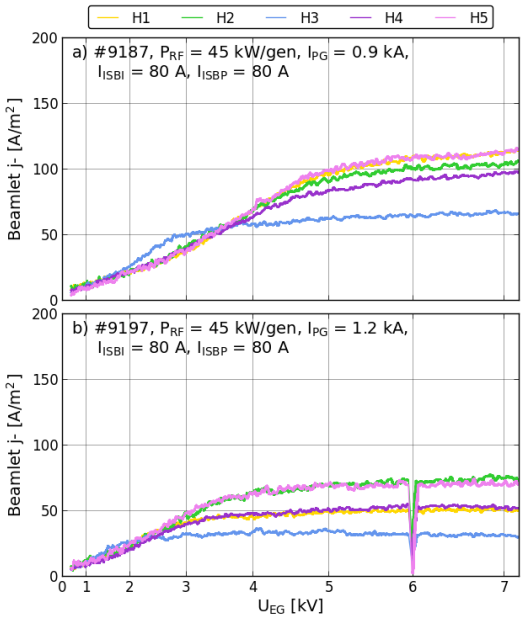

Figure 10. BCM beamlet currents for extraction voltage scans at two different plasma grid currents. A breakdown occurred during pulse 9197.

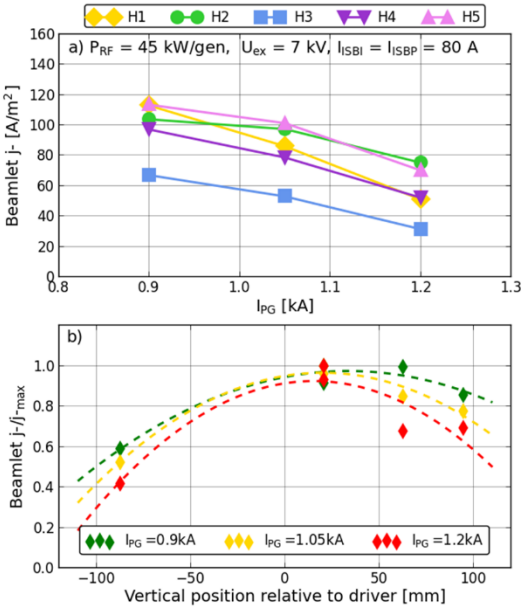

Figure 11. a) BCM beamlet current with increasing PG current and b) normalised current against vertical position relative to nearest driver.

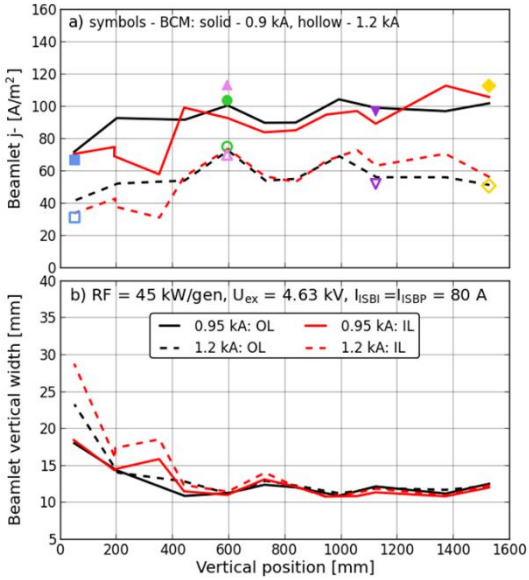

Figure 12. a) STRIKE current and b) beamlet vertical width profiles on the inner (black) and outer (red) left tiles (looking to the source) for high and low PG current cases from Figure 11. Compared to BCM currents at 7 kV (coloured markers based on sensor location as in Figure 1).

5 Improving homogeneity

The beam non-uniformity, in particular the top-bottom non-uniformity, is a direct consequence of non-uniformities in the plasma at the PG. This is seen in the spatially resolved source diagnostics, as described by Serianni et al [9]. Steps taken to improve the plasma uniformity, and the H^- availability, should therefore be apparent in the beamlet current.

5.1 Cs flux

To improve the availability of H^- in the bottom of the source, which is lower in the bottom segment, the Cs evaporation rate was increased from 6 mg/h to 24 mg/h. This results in an increase in the beamlet current at the bottom of the source (Figure 13, blue points for beamlet H3) as n_{H^-} increases. The other beamlets experience a smaller increase moving up the source. This may be due to U_{ex} not being high enough to fully extract all the available H^- at the top of the source. However, estimates of n_{H^-} at the PG and BP have shown that at the top of the source n_{H^-} increases at the BP instead of the PG as the Cs flux is increased [9]. This implies that the H- may move away from the PG into the expansion chamber instead of increasing further at the PG.

5.2 RF power unbalancing

Increasing the H- availability was also done by unbalancing the RF power of the generators, so that the segments with lower current would experience an increase in plasma density. Raising the RF power from 45 kW to 80 kW in the bottom segment results in a more homogeneous beamlet current distribution (Figure 14).

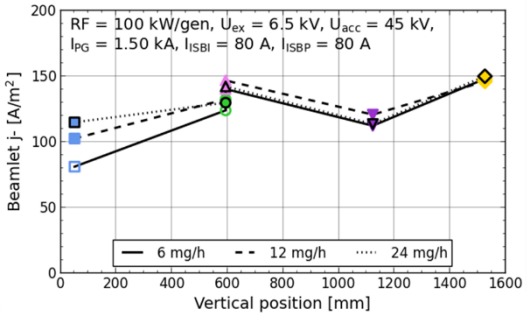

Figure 13. BCM beamlet current vertical profile for different Cs fluxes. Coloured markers based on sensor location as in Figure 1.

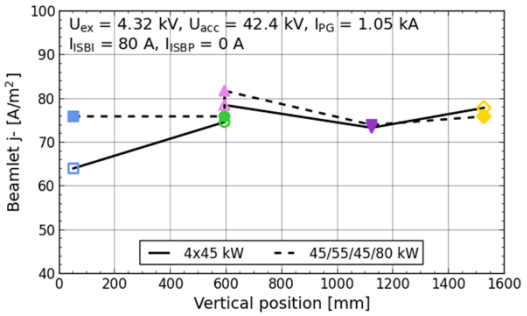

Figure 14. BCM beamlet current vertical profile for equal and unequal driver RF powers. Coloured markers based on sensor location as in Figure 1.

6 Conclusion

Using the beamlet current monitors a picture of the SPIDER beamlet current homogeneity has been obtained. Vertical top-bottom asymmetries in the plasma near the plasma grid, due to magnetic drifts, are reflected in the beamlet current. Increasing the bias increases the overall non-uniformity. The cause of the drifts, the transverse filter field, also results in an inhomogeneity on the beamlet group scale, with higher currents at the centre of the beamlet groups. The inhomogeneites, both global and local to the beamlet groups, have been confirmed with IR calorimetry.

Future operation of the SPIDER source with reduced apertures is planned, with solid-state RF amplifiers allowing 200 kW/generator and acceleration voltages greater than 60 kV. An enhanced number of DC beamlet current sensors, up to 15, will allow a spatially more detailed study of beam current uniformity.

7 Acknowledgments

This work has been carried out within the framework of the ITER-RFX Neutral Beam Testing Facility (NBTF) Agreement and has received funding from the ITER Organization. The views and opinions expressed herein do not necessarily reflect those of the ITER Organization.

This work has been carried out within the framework of the EUROfusion Consortium, funded by the European Union via the Euratom Research and Training Programme (Grant Agreement No

101052200 — EUROfusion). Views and opinions expressed are however those of the author(s) only and do not necessarily reflect those of the European Union or the European Commission. Neither the European Union nor the European Commission can be held responsible for them.

This work was supported in part by the Swiss National Science Foundation.

8 References

[1] V Toigo et al, The PRIMA Test Facility: SPIDER and MITICA test-beds for ITER neutral beam injectors, New J. Phys. 19 (2017) 085004. https://doi.org/10.1088/1367-2630/aa78e8

[2] G. Serianni et al, SPIDER in the roadmap of the ITER neutral beams, Fusion Eng. Des. 146 (2019), 2539-2546. https://doi.org/10.1016/j.fusengdes.2019.04.036

[3] Y. I. Belvenko, G. I. Dimov, V. G. Dudnikov, A powerful injector of neutrals with a surface-plasma source of negative ions, Nucl. Fusion 14 (1974) 113. https://doi.org/10.1088/0029-5515/14/1/017

[4] M. Pavei et al, SPIDER plasma grid masking for reducing gas conductance and pressure in the vacuum vessel, Fusion Eng. Des. 161 (2020) 112036. https://doi.org/10.1016/j.fusengdes.2020.112036

[5] A. Pimazzoni et al., Assessment of the SPIDER beam features by diagnostic calorimetry and thermography, Rev. Sci. Instrum. 91 (2020) 033301. https://doi.org/10.1063/1.5128562

[6] A. Shepherd et al, Initial Results from the SPIDER Beamlet Current Diagnostic, IEEE Trans. Plasma Sci. https://doi.org/10.1109/TPS.2022.3176757

[7] CSTR 0.3-P, https://www.lem.com/en/ctsr-03p (accessed 25 August 2022).

[8] E. Sartori et al, First operations with caesium of the negative ion source SPIDER, Nucl. Fusion 62 (2022) 086022. https://doi.org/10.1088/1741-4326/ac715e

[9] G. Serianni et al, Spatially-resolved diagnostics for optimisation of large ion beam sources, Rev. Sci. Instrum. 93 (2022) 081101. https://doi.org/10.1063/5.0084797

[10] A. Pimazzoni et al, Co-extracted electrons and beam inhomogeneity in the large negative ion source SPIDER, Fusion Eng. Des. 168 (2021) 112440. https://doi.org/10.1016/j.fusengdes.2021.112440